

Red Supergiant Stars within the Local Group

Lee. R. Patrick



Doctor of Philosophy
The University of Edinburgh
March 2016

Chapter 1

First steps outside the Local Group of Galaxies: Red Supergiants in NGC 55

1.1 Opening Remarks

To improve the quality of the data reduction I enlisted the help of a fellow student, Owen Turner, who has provided some additional corrections to the standard KMOS/esorex pipeline to correct for the readout bias and to improve the pipeline's bad pixel map. Details of this procedure are given in the text and the reader is referred to Turner et al. (in prep) for a more in depth discussion of the steps taken.

1.2 Introduction

NGC 55 is a galaxy located outside of the Local Group of Galaxies within the Sculptor Group at a distance of 1.94 ± 0.03 Mpc (Pietrzyński et al., 2006; Gieren et al., 2008) which, before the emergence of the Araucaria Project (Gieren et al., 2005), had been subject to considerable uncertainty (e.g. Pritchett et al., 1987; van de Steene et al., 2006).

The Sculptor Group is considered to be the closest group of galaxies to our

own and offers a fantastic laboratory with which to test theories of stellar and galactic evolution as using an 8-m class telescope, one can resolve individual stars within this group. Association to the Sculptor group however, is a contentious issue. Distance estimates vary to each galaxy, but typically when one references this group the main galaxies associated to this reference are: NGC 55, NGC 247, NGC 253, NGC 300 and NGC 7793. Where NGC 253 is a large starburst galaxy which is the brightest and most dominant galaxy within this group. In addition to these five large spiral galaxies, there are also numerous (~ 20) dwarf galaxies associated to this group.

By revising distances for nine of these dwarfs Karachentsev et al. (2003) postulated that the Sculptor group was actually more like a filament of galaxies, which intersects the Milky Way group, where NGC 55 and NGC 300 and their surrounding satellite galaxies were potentially not associated with the main group of galaxies in this filament. Regardless of the geometry and association to the Sculptor Group, NGC 55 is the nearest large galaxy to the MW group in the direction of the Sculptor Group.

The morphology of NGC 55 is asymmetric and complicated owing to the high inclination angle (up to 80° ; Hummel, Dettmar & Wielebinski, 1986; Westmeier, Koribalski & Braun, 2013). de Vaucouleurs (1961) classified this galaxy as an LMC-like spiral barred galaxy (SB(s)m) where the bar is seen along the line of sight de Vaucouleurs (1961) prompting various claims that this galaxy is an edge on analogue of the LMC (e.g. Robinson & van Damme, 1964, although not cited heavily – two citations in 50 years – the idea has propagated). Figure 1.1 shows NGC 55 and its complicated morphology where one can see the edge-on disk along the major axis of the galaxy and the brighter central part of the galaxy represents the head of the bar. In addition, to NGC 55 being orientated nearly edge on, extending from the disk-bar system there exists many star formation features such as giant H II regions as well as supergiant filaments and shells which are thought to allow ionising radiation to be transported to the halo where star-formation is currently occurring (Ferguson, Wyse & Gallagher, 1996).

The morphology of NGC 55, as well as its known population of massive hot stars (Castro et al., 2008, 2012), points to a recent history of intense star formation. This is supported by the infrared morphology of NGC 55 which is dominated by young star forming features (Engelbracht et al., 2004, with a star formation rate of $0.22 \text{ M}_\odot \text{yr}^{-1}$) as well as indications from near-IR imaging (Davidge, 2005).



Figure 1.1 *Image of NGC 55 where the edge on disk of the galaxy makes up the major axis and the bright central region represents the head of the bar containing intense star forming regions. Image from the Wide Field Imager on the 2.2-metre MPG/ESO telescope at ESO La Silla Observatory. Credit: ESO, press release.*

The metal content of NGC 55 is expected to be LMC-like, which is supported by Castro et al. (2012) who measured metallicities of 12 blue supergiants using optical spectroscopy and found a mean metallicity $[Z] = -0.40 \pm 0.13$ dex. In addition, Webster & Smith (1983) measure abundances of seven H II regions across the disk of NGC 55 using the strong-line method (as well as four measurements of the auroral “direct” line method) and found a similar LMC-like metallicity.

Even though the hot massive star population of NGC 55 has been explored, there currently exists no confirmed RSGs in NGC 55, although Davidge (2005) note that the near-IR CMDs of fields within the disk of NGC 55 reveal signatures of RSGs. This study represents the first quantitative study of RSGs in NGC 55 and, by measuring metallicities of this population, will provide a crucial test of the metallicity gradient within this galaxy.

In this chapter I describe the observations undertaken in Section 1.3 and highlight the target selection method and its uncertainties. Section ?? details the data reduction process and its complications owing to the poor S/N ratios of the observations. I then present the main results of the chapter in Section 1.5 where I first measure radial velocities for each epoch of the RGSs, confirming their

membership to NGC 55, and then go on to measure stellar parameters for each target using the *J*-band analysis technique described in detail in Chapter ???. Section 1.6 presents a discussion of the results and the main conclusions are presented in Section 1.7.

1.3 Observations

1.3.1 Target Selection

Targets were selected based on the optical photometry from the ACS Nearby Galaxy Survey Treasury (blue; ANGST Dalcanton et al., 2009) project. The optical CMD which is used to select targets is displayed in Figure 1.3, where the RSG candidates are within the black box and the observed targets are highlighted in red. This method of target selection is preferred as a result of the limited extent of near-IR photometry in this area. The ANGST project publicly available photometry for several fields within the disk of NGC 55 that are displayed as small white squares in Figure 1.2, overlaid on a DSS image. In addition to the ANGST HST photometry, ground-based optical photometry is obtained from the Araucaria Project which covers the full spatial extent of NGC 55 (large white rectangles in Figure 1.2).

The selection criteria used in this study makes is based optical $F606 - F814$ colours and $F814$ magnitudes. Owing to their cool temperatures and extreme luminosities RSGs are known to exist in a “plume” at the tip of a structure of cool stars in the $F606 - F814$, $F814$ CMD (e.g. Gazak et al., 2015). Figure 1.3 displays this CMD and the region of parameter space where RSG candidates reside is marked with a grey box. This box has the limits $17 < F814 < 19$ and $1.2 < F606 - F814 < 3.5$ following Gazak et al. (2015), where the faint magnitude limit is chosen to select only targets which will have a $S/N = 100$ in the original observing proposal. As with selection criteria in the near-IR, the lower limit of this criteria is contaminated with a population of super-AGB stars which can have luminosities comparable to the faintest RSGs (e.g. Nikolaev & Weinberg, 2000). However, as stated in Chapter ?? these stars are known to have lifetimes similar to the lowest mass RSGs and arguably still trace the young stellar population of this galaxy.

Table 1.1 shows ground- and space-based optical photometry of the KMOS targets

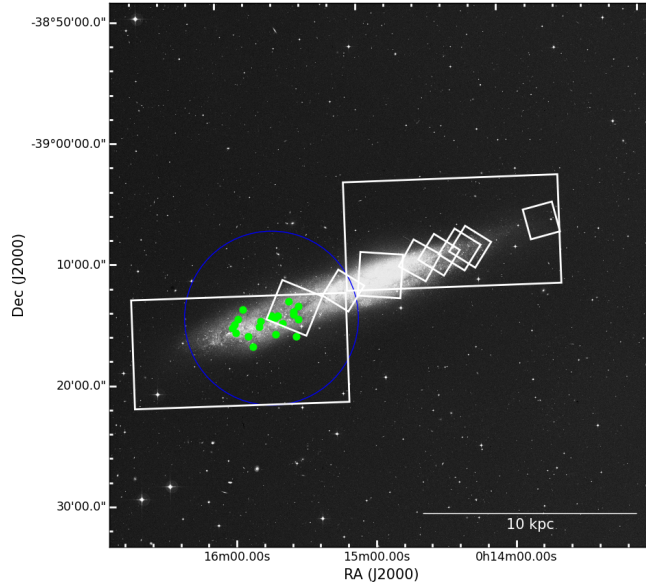


Figure 1.2 DSS image of NGC 55 with KMOS targets overlaid in green and photometric footprints from the Araucaria Project (Gieren et al., 2005) in white rectangles and the ANGST project (Dalcanton et al., 2009) in the smaller white squares.

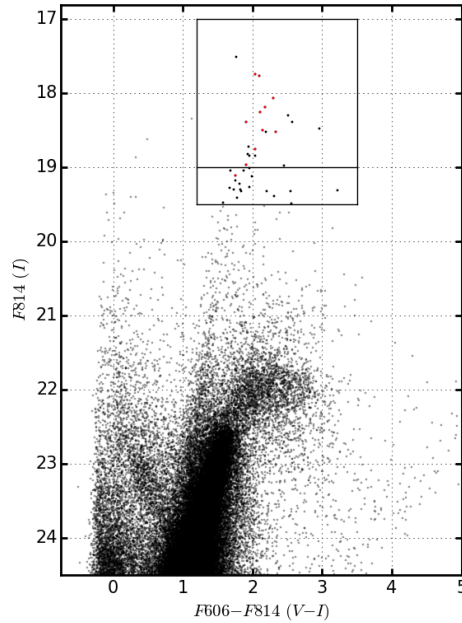


Figure 1.3 NGC 55 $V - I$ colour-magnitude diagram from the ACS Nearby Galaxy Survey Treasury (ANGST Dalcanton et al., 2009) project. The black box defines the selection criteria for candidate RSGs, which is defined as $17 < F814 < 19$ and $1.2 < F606 - F814 < 3.5$. The lower-panel of the black box defines priority 2 RSG candidates.

along with their radial velocities which confirm many of these targets as NGC 55 RSGs (see Section 1.5.1).

1.4 Observations and Data Reduction

These observations are part of the the KMOS guaranteed time observations (GTO) (ESO ID: 092.B-0088(A)) that was proposed to measure spatial variations in metallicities NGC 55 and NGC 300 both at $d = 1.9\text{Mpc}$. This included three pointings in NGC 55 containing ~ 60 RSG candidates. However, during the observations in October 2013, as a result of poor conditions, only half the requested time on one field in NGC 55 was observed. In order to supplement this partially completed OB, the proposal was re-submitted as a back-up OB for subsequent GTO.

As back-up observations, this OB was observed on two nights in August 2014. Therefore, this OB was observed on four different nights: 14-10-2013, 16-10-2013, 14-09-2014 and 15-10-2014 as detailed by Table 1.2. The observations on each night consisted of science exposures (O) with sky offset exposures (S) interveaved in an O, S, O observing pattern, where each exposure is 600 s.

In addition , on each night a standard set of KMOS calibration files was obtained as well as standard star observations on each night. In October 2013 HIP 3820 (B8 V; Houk, 1978) was observed using the 24-arm telluric template (KMOS_spec_acq_stdstarscipatt). However, on 14-10-2013, this OB was interrupted and several of the IFUs (particularly on detector two) were not observed with the 24-arm recipe: this OB was not repeated.

In August 2014 the 3-arm telluric tempate (KMOS_spec_cal_stdstar) was ob-servsed as opposed to the full 24-arm template. However, on both of these nights both HIP 3820 and HIP 18926 (B3 V; Houk & Smith-Moore, 1988) were observed as a standard star.

The quality of the observations taken on each night varies significantly. The first set of observations (14-09-2013) were taken in excellent conditions where the seeing conditions were stable with good transparency. As one would expect with back-up observations the conditions were not so idilic. On both nights where this OB was observed as a back-up target, the conditions were varying significantly thoughout the night wtih patchy, sometimes significant, cloud coverage.

Table 1.1 Summary of *VLT-KMOS* targets in *NGC 55*.

ID	S/N	α (J2000)	δ (J2000)	V ^a	I ^a	F606 ^b	F814 ^b	$\langle rv \rangle$ (km s ⁻¹)			Notes
								14-09-2013	16-10-2013	14-09-2014	
NGC55-RSG19	xx	00:15:29.190	-39:14:08.20	19.914	17.731	19.85	17.76	205±4	178±7	191±7	199±14
NGC55-RSG20	xx	00:15:29.520	-39:15:13.00	20.832	18.952	20.86	19.11	194±14	220±5	-	217±10
NGC55-RSG22	xx	00:15:30.520	-39:16:36.70	20.406	18.589	-	18.38	95±14	-41±26	-	Notes
NGC55-RSG24	xx	00:15:31.460	-39:14:46.30	20.612	18.475	20.29	18.38	186±6	194±7	146±38	192±16
NGC55-RSG25	xx	00:15:31.490	-39:14:32.40	20.316	18.394	20.63	18.49	204±12	217±16	-376±41 ^c	151±23
NGC55-RSG26	xx	00:15:33.160	-39:13:42.00	20.572	17.964	20.35	18.06	174±9	173±8	-	200±26
NGC55-RSG28	xx	00:15:36.160	-39:15:29.40	21.001	18.892	20.87	18.97	233±17	161±20	-	173±1
NGC55-RSG30	xx	00:15:38.030	-39:14:50.20	20.867	18.730	20.79	18.75	212±10	215±10	-424±21 ^c	203±41
NGC55-RSG35	xx	00:15:39.260	-39:15:01.70	20.007	17.872	19.78	17.73	202±3	206±4	223±13	213±2
NGC55-RSG36	xx	00:15:39.520	-39:16:23.10	19.915	18.462	-	-	-188±31	-284±16	-588±35	204±5
NGC55-RSG39	xx	00:15:40.260	-39:15:01.00	19.654	17.970	20.36	18.19	206±11	192±5	-1±30 ^c	-
NGC55-RSG43	xx	00:15:40.700	-39:14:50.20	19.957	18.183	20.36	18.25	-220±20 ^c	196±5	173±17	193±14
NGC55-RSG46	xx	00:15:41.640	-39:14:58.80	21.591	18.441	20.85	18.52	228±5	195±6	-128±18 ^c	194±9
NGC55-RSG57	xx	00:15:45.590	-39:15:16.40	20.010	18.220	-	-	217±10	197±6	206±11	Notes
NGC55-RSG58	xx	00:15:46.270	-39:15:43.20	20.619	18.400	-	-	236±8	216±3	214±21	Notes
NGC55-RSG60	xx	00:15:49.180	-39:17:19.80	21.393	18.847	-	-	-73±39	26±26	-533±39	218±8
NGC55-RSG65	xx	00:15:51.250	-39:16:26.40	19.706	17.653	-	-	224±5	215±4	94±37	-
NGC55-RSG67	xx	00:15:53.110	-39:14:13.60	19.925	18.047	-	-	25±24 ^c	217±6	218±4	Notes
NGC55-RSG69	xx	00:15:55.280	-39:15:00.10	20.470	18.666	-	-	231±5	195±9	130±14 ^c	193±16
NGC55-RSG70	xx	00:15:56.310	-39:16:08.60	22.300	18.907	-	-	155±12	187±9	202±20	222±18
NGC55-RSG71	xx	00:15:56.900	-39:15:27.50	20.401	18.559	-	-	197±11	214±11	320±16 ^c	180±20
NGC55-RSG73	xx	00:15:57.710	-39:15:41.50	20.489	18.411	-	-	161±7	178±6	-476±42 ^c	206±12
								136±35	136±35	176±19	171±11

^a Ground based data from the Araucaria Project Pietrzynski et al. (2006), with typical photometric uncertainty 0.075 and 0.016 in V and I bands respectively.

^b HST ANGST photometry from Dalcanton et al. (2009), with typical errors 0.12, 0.13 in F606 and F814 bands respectively.

^c Value excluded from average for target.

Table 1.2 *NGC 55 observing log.*

Date	Seeing Conditions (<i>arcsec</i>)	Airmass	Number of Exposures	Notes
14-10-2013	0''.8–1''.2	1.0–1.8	6 × 600s	Observed by author
16-10-2013	0''.8–1''.2	1.0–1.3	14 × 600s	Observed by author
14-09-2014	0''.4–2''.2	1.0–1.9	24 × 600s	Back-up observations
15-09-2014	1''.1–1''.6	1.1–1.5	12 × 600s	Back-up observations

Table 1.3 *Measured velocity resolution and resolving power across each detector.*

Date	Det.	IFUs	Ne $\lambda 1.17700 \mu\text{m}$		Ar $\lambda 1.21430 \mu\text{m}$	
			FWHM (km s $^{-1}$)	R	FWHM (km s $^{-1}$)	R
14-10-2013	1	1-8	95.48 ± 2.42	3140 ± 80	90.71 ± 2.09	3305 ± 76
	2	9-16	88.67 ± 1.67	3381 ± 64	86.35 ± 1.84	3472 ± 74
	3	17-24	82.89 ± 1.81	3617 ± 79	80.56 ± 2.11	3721 ± 97
16-10-2013	1	1-8	95.48 ± 2.46	3140 ± 81	90.78 ± 2.12	3302 ± 77
	2	9-16	88.91 ± 1.66	3371 ± 63	86.30 ± 1.85	3473 ± 74
	3	17-24	82.96 ± 2.14	3612 ± 76	80.77 ± 2.14	3712 ± 98
14-09-2015	1	1-8	84.18 ± 1.93	3561 ± 82	81.76 ± 2.15	3667 ± 96
	2	9-16	87.00 ± 1.69	3446 ± 67	84.67 ± 1.93	3541 ± 81
	3	17-24	97.14 ± 1.88	3086 ± 60	94.85 ± 2.01	3161 ± 67
15-09-2014	1	1-8	82.55 ± 1.96	3632 ± 86	80.41 ± 2.30	3728 ± 106
	2	9-16	88.08 ± 1.78	3404 ± 69	86.03 ± 1.96	3485 ± 80
	3	17-24	98.04 ± 1.91	3058 ± 59	96.74 ± 2.05	3099 ± 66

These differences in the quality of the data and in the actual execution of the observations must all be taken into account when the data is reduced. In addition to differences in the observations arising from the conditions, there are also differences as a result of the time between the observations. Table 1.3 shows the mean measured resolution and resolving power, at the appropriate rotator angles, for each night where the NGC 55 data were taken. This table shows that the resolution can vary significant between each night, particularly on detector three where the mean resolving power changes by a factor of 1/5. Therefore, this must be taking into consideration when combining exposures on different nights. This is solved by using a simple Gaussian filter (as first described in Chapter ??) to degrade the resolution of the spectra to that of the lowest resolution spectrum within the data set. For example, all spectra for a star in IFU 1 would be degraded to a resolution of 3302 (see Table 1.3) before being combined into a master spectrum for the four nights.

The observations were reduced using the recipes provided by the Software Package

for Astronomical Reduction with KMOS (SPARK; Davies, R. I. et al., 2013). The standard KMOS/esorex routines were used to calibrate and reconstruct the science and standard-star data cubes as outlined by Davies, R. I. et al. (2013) including a correction which corrects for the readout column bias as well as enhancing the bad pixel mask following Turner et al. (in prep.). Using the reconstructed data cubes the pipeline was used to extract science and sky spectra in a consistent way for all exposures.

Sky subtraction was performed using the ESO SKYCORR package (Noll et al., 2014). SKYCORR is an instrument independent tool that applies a scaling to a sky spectrum given a pair of observed and sky spectra in order to more accurately match the sky lines in the observed spectrum and hence, provide a more accurate sky subtraction. This works by adapting the reference sky spectrum to correct for differences as a result of temporal and spatial airglow variability. This software is specifically designed for observations at Cerro Paranal and has been shown to be an effective tool for various different science goals (e.g. Noll et al., 2014; Gazak et al., 2015; Fossati et al., 2016; La Barbera et al., 2016).

Telluric correction is performed on each sky subtracted spectrum (before combination) using the method described in full in Chapter ???. Briefly, additional corrections are made to the standard KMOS/esorex method of telluric correction by correcting for potential offsets between the wavelength solutions of the science and telluric spectra using a iterative cross-correlation approach. In addition, a simple scaling is applied to the telluric spectrum in order to more accurately match the telluric absorption in the science spectrum. Once these addition corrections have been implemented, I divide the science spectrum by the telluric using only the 1.16–1.21 μm region.

As mentioned above, during each night of observing at least one telluric standard-star was observed. Where multiple telluric spectra were available for a single science spectrum, all appropriate telluric spectra were used to apply the telluric correction. The spectra resulting from these corrections are then compared visually and the spectrum producing the fewest residuals is selected. There were instances where multiple spectra were of equal quality, in these cases both spectra were used in the combination process.

To combine the fully calibrated and corrected spectra on each night, I first degrade the spectral resolution of all spectra to the lowest resolution of the set as defined by Table 1.3. Once all spectra are at a constant resolution I

correct for any differences in the wavelength solution by using an iterative cross-correlation approach, where the spectra are all corrected to the rest frame of a single “reference” spectrum. The choice of the reference spectrum is important as if one selected a poor quality reference spectrum with strong sky- or telluric-correction residuals, this could result in an alignment of the residuals which would amplify these features when finally combined. To avoid this, the highest-quality spectrum for each target is selected as the reference spectrum. In practise, this was typically frame four of the night of 16-09-2013.

This procedure mainly corrects for differences in the wavelength solution from difference nights, typically on an individual night (particularly in the case of 14-09-2013 and 16-09-2013) there are not significant differenes in the wavelength solution. Once this correction is implemented all spectra are combined using a simple median combine. This simple method is preferred to something more sophisticated as there were significant sky- and telluric-correction residuals present in many of these spectra which are found to be most effectively extinguished using a median combination.

1.5 Results

1.5.1 Radial Velocities

Radial velocities are measured using the method described first in Chapter ?? where radial velocities are measured using several strong spectral features within the 1.16–1.21 μm region. Each of these spectral features is independently used to measure a radial velocity where the value quoted is the average of these measurements and the uncertainties are defined by the standard deviation of the measurements. This method is known to work well on KMOS stellar spectra Lapenna et al. (2015); Patrick et al. (2015, 2016).

Velocities are measured by combining frames from each night individually using the standard KMOS/esorex routines, rather than the method described above. Estimated radial velocities from each KMOS pointing is listed in Table 1.1 alongside the average radial velocity for each target, where any significantly discrepant measurement has been excluded as a result of residuals in the spectrum perturbing the fit (marked by note c in Table 1.1). This is a particular problem on the night of 14-09-2014 where 7/20 velocity measurements were

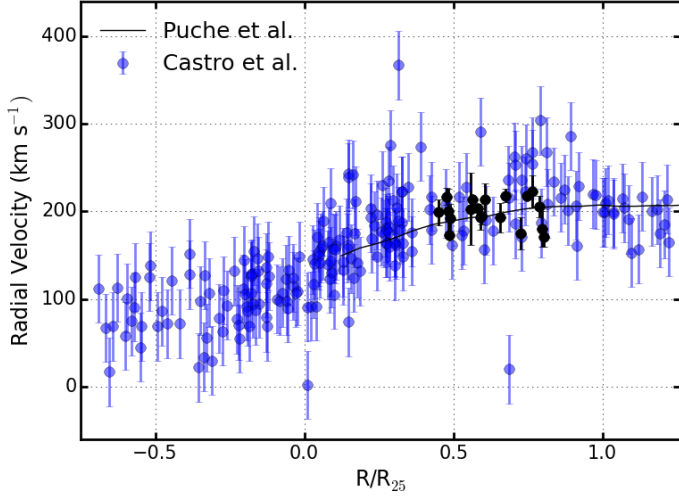


Figure 1.4 Radial velocities for the KMOS RSGs (black points) shown against projected radius from the centre of NGC 55 as defined by the Two Micron All Sky Survey (2MASS; Skrutskie et al., 2006) scaled by $R_{25} = 16.2 \pm 0.4$ arcmin (de Vaucouleurs et al., 1991). Blue points show data for ~ 200 BSGs in NGC 55 from (Castro et al., 2008, ; shown with 50% transparency to highlight densely populated areas) alongside the rotation curve of NGC 55 (black solid line; Puche, Carignan & Wainscoat, 1991).

excluded. Uncertainties quoted on the average are the standard deviation of the measurements on each night. Three targets (NGC55-RSG22, NGC55-RSG36 and NGC55-RSG60) have been excluded from this average based on their unreliable radial velocity estimates. Given the significant variability in these measurements on each night, an assessment on membership to NGC 55 is impossible given the current data. Therefore, henceforth, these targets are excluded from the sample.

Comparing the estimated velocities to previous measurements we find good agreement with velocities measured for ~ 200 BSGs in NGC 55 in (Castro et al., 2008) as well as with measurements of the velocity from the HI gas (Puche, Carignan & Wainscoat, 1991). The estimated radial velocities as a function of galactocentric distance is shown in Figure 1.4 where previous measurements are also shown for comparison. The radius at which the surface brightness first reach 25 mag/arcsec² in the *B*-band (R_{25} e.g. Schneider, 2015) is shown for scale ($R_{25} = 16.2 \pm 0.4$ arcmin de Vaucouleurs et al., 1991) We find no evidence for a systematic offset between the measurements of Castro et al. (2008) and those measured in this study.

As the observed data is taken over four different epochs, the variability of

each source can be assessed. No clear evidence for variability is found for any target within the observed sample. To assess variability, the variability criteria of (Hénault-Brunet et al., 2012) is employed, i.e.

$$\left| \frac{RV_i - \mu}{\sigma_i} \right| > 4.0, \quad (1.1)$$

where RV_i is the radial velocity with an associated uncertainty σ_i measured on an individual night i and μ is the average radial velocity for the target. Using this criteria on all targets finds that no targets show evidence for variability. This adds strength to the suggestion that observed RSGs are intrinsically single objects as a result of the length of time spent as a RSG in a binary is significantly decreased (see discussion in Chapter ??).

1.5.2 Stellar Parameters

Stellar parameters are estimated for each target using the J -band analysis technique detailed in Chapter ???. This analysis is used to measure stellar parameters, including overall metallicity – to a precision of ± 0.15 dex at the resolution of KMOS observations with $S/N \geq 100$. The parameter ranges are given shown in Chapter ??, Table ??.

The analysis uses synthetic RSG spectra, extracted from MARCS model atmospheres (Gustafsson et al., 2008), computed with corrections for non-local thermodynamic equilibrium for lines from titanium, iron, silicon and magnesium (Bergemann et al., 2012, 2013, 2015). The synthetic spectra are compared with observations using the χ^2 -squared statistic and the synthetic spectra are degraded to the resolution and sampling of the observations.

Estimated stellar parameters are listed in Table 1.4 and the best-fit model spectra are shown with the final reduced science spectra in Figure ???. Assuming no spatial variations in metallicity the average metallicity of of the sample is -0.36 ± 0.28 dex. This average value compares well to the average metallicity measured using 12 BSGs in NGC 55 from (Castro et al., 2012, -0.4 ± 0.13). These authors find no evidence for spatial variations in metallicity in NGC 55, however, recently, Kudritzki et al. (in prep) measure metallicities for ~ 60 BSGs in NGC 55 covering a larger spatial extent and find evidence for a metallicity gradient of xx.xx dex/kpc: the first detected in this galaxy.

Table 1.4 Physical parameters determined for the KMOS targets in NGC 55.

Target	IFU	ξ (km s $^{-1}$)	[Z]	$\log g$	T _{eff} (K)	Notes
NGC55-RSG19	6	–	–	–	–	
NGC55-RSG20	7	–	–	–	–	
NGC55-RSG22	11	–	–	–	–	
NGC55-RSG24	10	–	–	–	–	
NGC55-RSG25	8	3.2 ± 0.9	-0.53 ± 0.33	0.12 ± 0.36	3460 ± 250	
NGC55-RSG26	4	–	–	–	–	
NGC55-RSG28	5	–	–	–	–	
NGC55-RSG30	3	–	–	–	–	
NGC55-RSG35	12	4.1 ± 0.6	-0.35 ± 0.26	-0.13 ± 0.24	3750 ± 120	
NGC55-RSG36	9	–	–	–	–	
NGC55-RSG39	14	3.4 ± 0.7	-0.28 ± 0.28	-0.13 ± 0.25	3700 ± 100	
NGC55-RSG43	24	3.8 ± 0.8	-0.27 ± 0.26	0.12 ± 0.98	3960 ± 250	
NGC55-RSG46	22	–	–	–	–	
NGC55-RSG57	1	4.1 ± 0.7	-0.39 ± 0.28	0.10 ± 0.24	3550 ± 270	
NGC55-RSG58	15	–	–	–	–	
NGC55-RSG60	16	–	–	–	–	
NGC55-RSG65	17	–	–	–	–	
NGC55-RSG67	23	–	–	–	–	
NGC55-RSG69	21	–	–	–	–	
NGC55-RSG70	18	–	–	–	–	
NGC55-RSG71	20	–	–	–	–	
NGC55-RSG73	19	–	–	–	–	

Using a maximum likelihood MCMC parameter estimation for a linear fit to the metallicities measured for RSGs in NGC 55 I find (thus far) no evidence for spatial variations in metallicity (0.1 ± 0.1 dex/kpc).

- Comparison to previous results Castro et al. (2012) find average $[Z] = -0.4 \pm 0.13$ dex Z Vs. Radius from galaxy centre
- MCMC parameter estimation for the fit

1.6 Discussion

1.6.1 Orientation of NGC 55

1.6.2 Stellar Evolution

Luminosities have been calculated for the targets using the bolometric corrections of (?) where the F808 HST bandpass where available, otherwise the ground-based *I*-band filter has been used. Figure 1.7 shows a H-R diagram for these targets using the temperatures estimated in Section 1.5 along with SMC-like evolutionary tracks (Georgy et al., 2013).

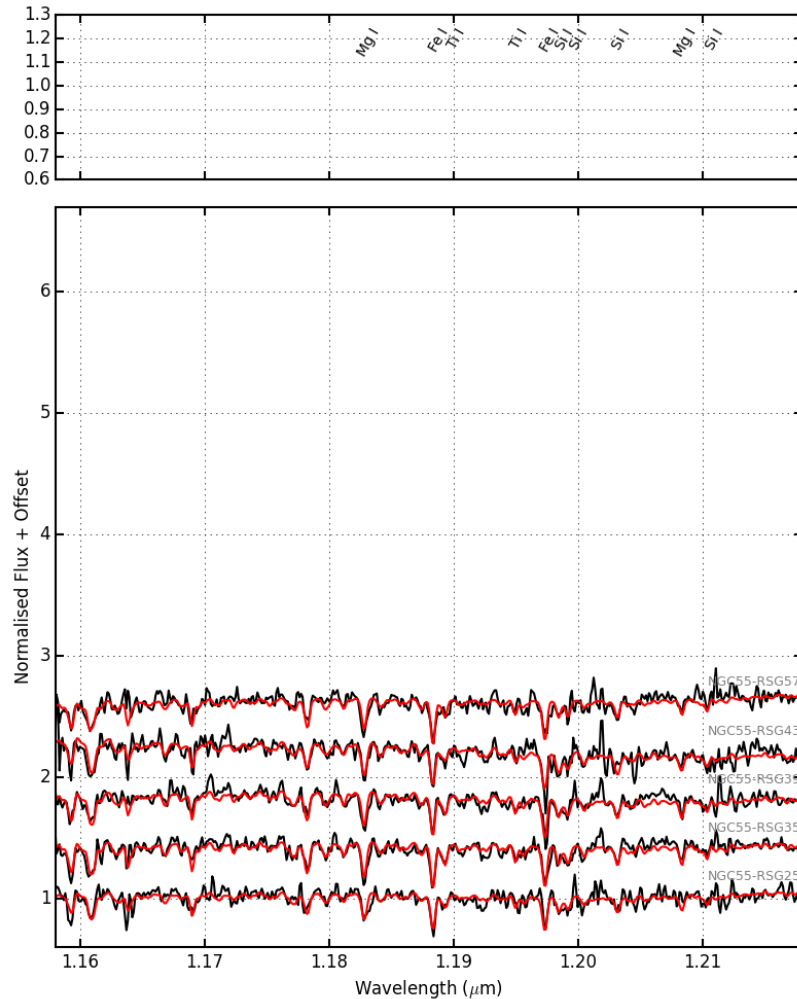


Figure 1.5 Observed and best-fit model spectra of RSGs in NGC55 (black and red lines, respectively). The lines used for the analysis, from left-to-right by species, are $Fe\,I\lambda\lambda 1.188285, 1.197305$; $Mg\,I\lambda\lambda 1.182819, 1.208335$; $Si\,I\lambda\lambda 1.198419, 1.199157, 1.203151, 1.210353$; $Ti\,I\lambda\lambda 1.189289, 1.194954$.

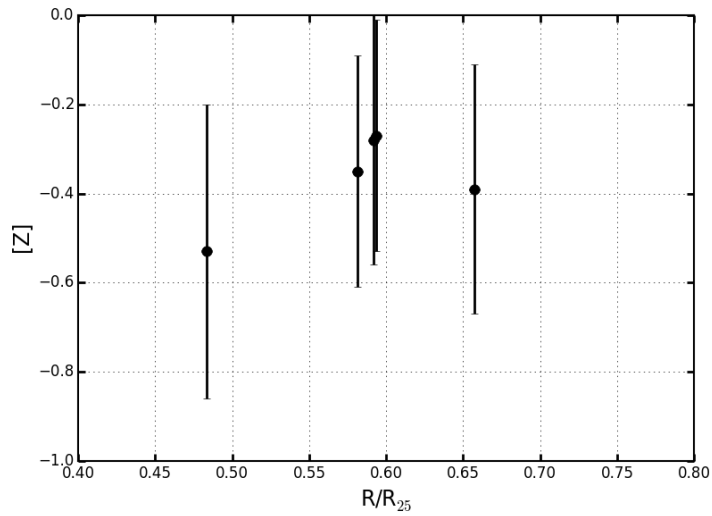


Figure 1.6 Metallicities for KMOS RSGs (black points) shown against projected radius from the centre of NGC 55 as defined by the Two Micron All Sky Survey (2MASS; Skrutskie et al., 2006) scaled by $R_{25} = 16.2 \pm 0.4$ arcmin (de Vaucouleurs et al., 1991).

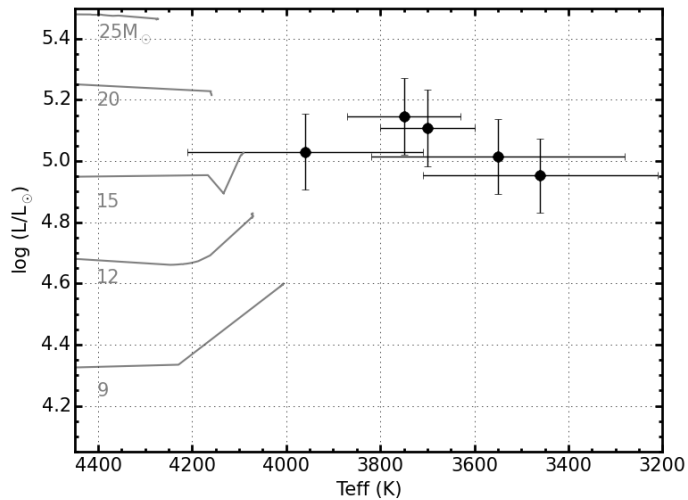


Figure 1.7 Hertzsprung–Russell diagram for NGC 55. Solid grey lines show SMC-like metallicity evolutionary models including rotation (Georgy et al., 2013).

1.7 Conclusions

Bibliography

- Bergemann M., Kudritzki R.-P., Gazak Z., Davies B., Plez B., 2015, ApJ, 804, 113
- Bergemann M., Kudritzki R.-P., Plez B., Davies B., Lind K., Gazak Z., 2012, ApJ, 751, 156
- Bergemann M., Kudritzki R.-P., Würl M., Plez B., Davies B., Gazak Z., 2013, ApJ, 764, 115
- Castro N. et al., 2008, A&A, 485, 41
- Castro N. et al., 2012, A&A, 542, A79
- Dalcanton J. J. et al., 2009, ApJS, 183, 67
- Davidge T. J., 2005, ApJ, 622, 279
- Davies, R. I. et al., 2013, A&A, 558, A56
- de Vaucouleurs G., 1961, ApJ, 133, 405
- de Vaucouleurs G., de Vaucouleurs A., Corwin, Jr. H. G., Buta R. J., Paturel G., Fouqué P., 1991, Third Reference Catalogue of Bright Galaxies. Volume I: Explanations and references. Volume II: Data for galaxies between 0^h and 12^h . Volume III: Data for galaxies between 12^h and 24^h .
- Engelbracht C. W. et al., 2004, ApJS, 154, 248
- Ferguson A. M. N., Wyse R. F. G., Gallagher J. S., 1996, AJ, 112, 2567
- Fossati M., Fumagalli M., Boselli A., Gavazzi G., Sun M., Wilman D. J., 2016, MNRAS, 455, 2028
- Gazak J. Z. et al., 2015, ApJ, 805, 182

- Georgy C. et al., 2013, A&A, 558, A103
- Gieren W. et al., 2005, The Messenger, 121, 23
- Gieren W., Pietrzyński G., Soszyński I., Bresolin F., Kudritzki R.-P., Storm J., Minniti D., 2008, ApJ, 672, 266
- Gustafsson B., Edvardsson B., Eriksson K., J rgensen U. G., Nordlund Å., Plez B., 2008, A&A, 486, 951
- Hénault-Brunet V. et al., 2012, A&A, 546, A73
- Houk N., 1978, Michigan catalogue of two-dimensional spectral types for the HD stars
- Houk N., Smith-Moore M., 1988, Michigan Catalogue of Two-dimensional Spectral Types for the HD Stars. Volume 4, Declinations -26deg.0to – 12deg.0.
- Hummel E., Dettmar R.-J., Wielebinski R., 1986, A&A, 166, 97
- Karachentsev I. D. et al., 2003, A&A, 404, 93
- La Barbera F., Vazdekis A., Ferreras I., Pasquali A., Cappellari M., Martín-Navarro I., Schönebeck F., Falcón-Barroso J., 2016, MNRAS, 457, 1468
- Lapenna E., Origlia L., Mucciarelli A., Lanzoni B., Ferraro F. R., Dalessandro E., Valenti E., Cirasuolo M., 2015, ApJ, 798, 23
- Nikolaev S., Weinberg M. D., 2000, ApJ, 542, 804
- Noll S., Kausch W., Kimeswenger S., Barden M., Jones A. M., Modigliani A., Szyszka C., Taylor J., 2014, A&A, 567, A25
- Patrick L. R., Evans C. J., Davies B., Kudritzki R., Hénault-Brunet V., Bastian N., Lapenna E., Bergemann M., 2016, ArXiv e-prints
- Patrick L. R., Evans C. J., Davies B., Kudritzki R.-P., Gazak J. Z., Bergemann M., Plez B., Ferguson A. M. N., 2015, ApJ, 803, 14
- Pietrzyński G. et al., 2006, AJ, 132, 2556
- Pritchett C. J., Schade D., Richer H. B., Crabtree D., Yee H. K. C., 1987, ApJ, 323, 79

- Puche D., Carignan C., Wainscoat R. J., 1991, AJ, 101, 447
- Robinson B. J., van Damme K. J., 1964, in IAU Symposium, Vol. 20, The Galaxy and the Magellanic Clouds, Kerr F. J., ed., p. 276
- Schneider P., 2015, Extragalactic Astronomy and Cosmology: An Introduction
- Skrutskie M. F. et al., 2006, AJ, 131, 1163
- Tanaka M., Chiba M., Komiyama Y., Guhathakurta P., Kalirai J. S., 2011, ApJ, 738, 150
- van de Steene G. C., Jacoby G. H., Praet C., Ciardullo R., Dejonghe H., 2006, A&A, 455, 891
- Webster B. L., Smith M. G., 1983, MNRAS, 204, 743
- Westmeier T., Koribalski B. S., Braun R., 2013, MNRAS, 434, 3511

Bibliography

- Bergemann M., Kudritzki R.-P., Gazak Z., Davies B., Plez B., 2015, ApJ, 804, 113
- Bergemann M., Kudritzki R.-P., Plez B., Davies B., Lind K., Gazak Z., 2012, ApJ, 751, 156
- Bergemann M., Kudritzki R.-P., Würl M., Plez B., Davies B., Gazak Z., 2013, ApJ, 764, 115
- Castro N. et al., 2008, A&A, 485, 41
- Castro N. et al., 2012, A&A, 542, A79
- Dalcanton J. J. et al., 2009, ApJS, 183, 67
- Davidge T. J., 2005, ApJ, 622, 279
- Davies, R. I. et al., 2013, A&A, 558, A56
- de Vaucouleurs G., 1961, ApJ, 133, 405
- de Vaucouleurs G., de Vaucouleurs A., Corwin, Jr. H. G., Buta R. J., Paturel G., Fouqué P., 1991, Third Reference Catalogue of Bright Galaxies. Volume I: Explanations and references. Volume II: Data for galaxies between 0^h and 12^h . Volume III: Data for galaxies between 12^h and 24^h .
- Engelbracht C. W. et al., 2004, ApJS, 154, 248
- Ferguson A. M. N., Wyse R. F. G., Gallagher J. S., 1996, AJ, 112, 2567
- Fossati M., Fumagalli M., Boselli A., Gavazzi G., Sun M., Wilman D. J., 2016, MNRAS, 455, 2028
- Gazak J. Z. et al., 2015, ApJ, 805, 182
- Georgy C. et al., 2013, A&A, 558, A103
- Gieren W. et al., 2005, The Messenger, 121, 23
- Gieren W., Pietrzyński G., Soszyński I., Bresolin F., Kudritzki R.-P., Storm J., Minniti D., 2008, ApJ, 672, 266

- Gustafsson B., Edwardsson B., Eriksson K., J rgensen U. G., Nordlund Å., Plez B., 2008, A&A, 486, 951
- Hénault-Brunet V. et al., 2012, A&A, 546, A73
- Houk N., 1978, Michigan catalogue of two-dimensional spectral types for the HD stars
- Houk N., Smith-Moore M., 1988, Michigan Catalogue of Two-dimensional Spectral Types for the HD Stars. Volume 4, Declinations -26deg.0to – 12deg.0.
- Hummel E., Dettmar R.-J., Wielebinski R., 1986, A&A, 166, 97
- Karachentsev I. D. et al., 2003, A&A, 404, 93
- La Barbera F., Vazdekis A., Ferreras I., Pasquali A., Cappellari M., Martín-Navarro I., Schönebeck F., Falcón-Barroso J., 2016, MNRAS, 457, 1468
- Lapenna E., Origlia L., Mucciarelli A., Lanzoni B., Ferraro F. R., Dalessandro E., Valenti E., Cirasuolo M., 2015, ApJ, 798, 23
- Nikolaev S., Weinberg M. D., 2000, ApJ, 542, 804
- Noll S., Kausch W., Kimeswenger S., Barden M., Jones A. M., Modigliani A., Szyszka C., Taylor J., 2014, A&A, 567, A25
- Patrick L. R., Evans C. J., Davies B., Kudritzki R., Hénault-Brunet V., Bastian N., Lapenna E., Bergemann M., 2016, ArXiv e-prints
- Patrick L. R., Evans C. J., Davies B., Kudritzki R.-P., Gazak J. Z., Bergemann M., Plez B., Ferguson A. M. N., 2015, ApJ, 803, 14
- Pietrzyński G. et al., 2006, AJ, 132, 2556
- Pritchett C. J., Schade D., Richer H. B., Crabtree D., Yee H. K. C., 1987, ApJ, 323, 79
- Puche D., Carignan C., Wainscoat R. J., 1991, AJ, 101, 447
- Robinson B. J., van Damme K. J., 1964, in IAU Symposium, Vol. 20, The Galaxy and the Magellanic Clouds, Kerr F. J., ed., p. 276
- Schneider P., 2015, Extragalactic Astronomy and Cosmology: An Introduction
- Skrutskie M. F. et al., 2006, AJ, 131, 1163
- Tanaka M., Chiba M., Komiyama Y., Guhathakurta P., Kalirai J. S., 2011, ApJ, 738, 150
- van de Steene G. C., Jacoby G. H., Praet C., Ciardullo R., Dejonghe H., 2006, A&A, 455, 891

Webster B. L., Smith M. G., 1983, MNRAS, 204, 743

Westmeier T., Koribalski B. S., Braun R., 2013, MNRAS, 434, 3511